

# Spatio-Temporal Point Processes with Attention for Traffic Congestion Event Modeling

Shixiang Zhu, Ruyi Ding, Minghe Zhang, Pascal Van Hentenryck, Yao Xie

**Abstract**—We present a novel framework for modeling traffic congestion events over road networks based on new mutually exciting spatio-temporal point process models with attention mechanisms and neural network embeddings. Using multi-modal data by combining count data from traffic sensors with police reports that report traffic incidents, we aim to capture two types of triggering effect for congestion events. Current traffic congestion at one location may cause future congestion over the road network, and traffic incidents may cause spread traffic congestion. To capture the non-homogeneous temporal dependence of the event on the past, we introduce a novel attention-based mechanism based on neural networks embedding for the point process model. To incorporate the directional spatial dependence induced by the road network, we adapt the “tail-up” model from the context of spatial statistics to the traffic network setting. We demonstrate the superior performance of our approach compared to the state-of-the-art methods for both synthetic and real data.

## I. INTRODUCTION

Traffic congestion modeling is critical to modern transportation applications, such as route guidance or traffic network planning. For example, in Atlanta, which has over half a million daily commuters, reducing congestion is a top priority, and the city spends millions of dollars on traffic-reducing measures, including toll lanes and high-capacity transport [1]. However, modeling the complex traffic dynamics and predicting traffic congestion events in real-time is vital but has remained extremely challenging. Indeed, traffic modeling is inherently intricate because of the complex spatio-temporal dynamics and the fact that congestion also stems from responses to real-time random events, such as police interventions and traffic accidents. As a result, understanding and predicting congestion events can help cities to plan traffic more efficiently and plan for future urban development.

Traffic sensors distributed over highway and road networks are widely deployed: They are a key technology enabler that provides a unique opportunity to understand the traffic dynamic and congestion. Traffic sensor data reports traffic counts, i.e., the number of cars passing through per unit of time. These traffic counts are exploited by most existing work (reviewed in the section below), but traditional approaches do not model traffic events and incidents, which are fundamentally different in nature. An important feature of traffic congestion modeling is the ability to capture *triggering effects*. For example, when congestion occurs, the effect will propagate, and subsequent congestion is typically more likely to happen along the affected road or highway. Moreover, other types of events, such as

police interventions, may also trigger traffic congestion. Such events, which are logged in police report data, provide an additional source of data that may be useful for modeling and predicting traffic congestion.

In this paper, we aim to capture these two types of events and their triggering effect. Hawkes processes (also called self-exciting point processes) are a popular model for modeling such a triggering effect, and they have been successfully used in many different applications (see [2] for a review). A Hawkes process models the dependence between events using mutually dependent point processes, with intensities depending on historical events.

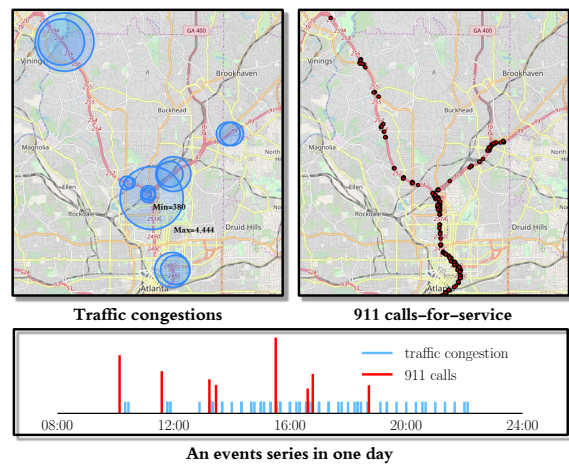


Fig. 1: An overview of the Atlanta traffic dataset. **Left** shows the numbers of traffic congestions recorded by 14 traffic sensors. The size of the blue bubble represents the total number of traffic congestion events recorded by one traffic sensor. **Right** shows the spatial distribution of traffic incidents reported by 911 calls on the highway. Black dots represent the locations of traffic incidents. **Bottom** An event series in a single day. The height of the red bar indicates the length of the processing time.

There are two main reasons for the knowledge gap between existing point process models and our application in traffic congestion event modeling. (1) Most existing models assume that the influence function *decays monotonically* over time and space and introduce parametric models for the influence function. For instance, this approach is used in methods based on the popular Recurrent Neural Networks (RNNs) [3], [4], [5], [6], [7], [8], [9], which have achieved various successes in modeling complex temporal dependence: e.g., [3] assumes that the influence of an event decreases or increases exponentially over time. However, in traffic modeling settings, the influence

of past events may not decay monotonically over time or space. For example, suppose that a bad car accident occurs on the highway. The police will be called to the scene and may need to wait for a specialized unit, like a crane, to come to move the wreckage. This could take several hours. Meanwhile, the whole highway would be shut down, and the event’s influence would not decay at all. (2) We need to consider the specific spatial correlation structure induced by road networks in our modeling. Most Hawkes process models focus on temporal modeling or discretizing space and treat it as a multi-dimensional Hawkes process. However, it is critical to embed the special spatial correlation induced by the model’s road networks. Indeed, the spatial dependence is highly *directional* and what happens “up-stream” will influence what happens “down-stream”, and the sensors along the same road (in the same direction) will have higher correlations.

In this paper, we aim at filling this gap by presenting a novel attention mechanism based point processes (APP) model that reveals an analytical relationship between endogenous and exogenous factors for traffic congestion. Specifically, we consider the police intervention as *exogenous promotion* [10] on traffic congestion and consider the influence between congestion events as *endogenous self-excitation*. The dynamics of the endogenous self-excitation can be captured via the so-called *attention* mechanism. The attention mechanism [11], [12] is originally proposed to capture the non-linear dependence between words in Natural Language Processing. To capture the complex non-homogeneous influence of historical events on the future, we go beyond the assumption that the influence of the historical event fades over time, and leverage the attention mechanism to develop a flexible framework that “focuses” on past events with high importance score on the current event. We introduce an adaptive *score function* to measure the importance between past events and the current event, which extends the conventional dot-product score [12] used in other attention models and is highly interpretable. To tackle the directional spatial correlation induced by road networks, we also adopt the idea of the “tail-up” model (developed for spatial statistics for Gaussian processes) to our point process setting. Finally, to achieve constant memory in the face of streaming data, we introduce an online algorithm to efficiently implement our APP model’s attention component, where only the most informative events in the past are retained for computation. Using experiments based on real data, we show that our proposed method outperforms the state-of-the-art both in maximizing the likelihood function of a point process compared with previous approaches and in prediction accuracy on a real-data traffic data set from Atlanta.

The main contributions of our paper are as follows. (1) To the best of our knowledge, our APP model is the first attempt to combine traffic sensor count data with police reports for traffic event modeling. (2) In terms of methodology, our APP model includes a novel attention-based mechanism to capture a non-homogeneous spatio-temporal dependence of the event on the past. (3) The APP model includes a novel approach to capture the directional spatial dependence by adapting a similar idea used for the “tail-up” model, which was used to model spatial correlation for hydrology systems such as

rivers and streams. (4) Our experimental results demonstrate the benefits of the APP model both on synthetic and real case studies.

**Related work.** Most of the previous works [13], [14], [15], [16], [17], [18], [19], [20], [21], [22] on traffic modeling focus on predicting speed, volume, density and travel time, which have achieved remarkable success in this field. Other works [23], [24], [25] target at modeling traffic congestion based on the speed, and density of vehicle stream, which gives good mathematical descriptions for traffic flow. However, dynamic traffic event modeling is a new approach and still in the nascent stage. Existing work in discrete event modeling using point processes, such as [26], [27], [28], [29], often make strong assumptions and specify a parametric form of the intensity functions. Such methods enjoy good interpretability and are efficient. However, parametric models are not expressive enough to capture the event dynamics in some applications.

Recent interest has focused on improving the expressive power of point process models. There are have been attempts on RNNs based point process models [3], [4], [7], [9], which use RNNs to memorize the influence of historical events. However, the conditional intensity is assumed to be some specific functional forms. There are other attempts [5], [8] in using RNNs to model event dependence without specifying the conditional intensity function explicitly. These works only use RNN as a generative model where the conditional function is not available. They focus on studying different learning strategies since maximum likelihood estimation is not applicable here.

Another recent work [30] has aimed at looking for a more general way to model point processes, where no parametric form is assumed. It uses a neural network to parameterize the hazard function, where the conditional intensity can be further derived by taking the derivative of the hazard function. This approach is highly flexible and easy to compute since no numerical integral calculation is involved. However, the model is only specified using a neural network, which reduces interpretability. In addition, this model only works for temporal events.

A recent work [31] also uses attention to model the historical information in point processes. However, their proposal differs from our APP model because it is still a parametric form and assumes a decaying exponential assumption on the conditional intensity function, which may not capture distant events although they are important. We do not make such assumptions in our APP model and can capture important events as long as their “importance score” is high. Moreover, [31] focuses on temporal point processes while we also consider spatio-temporal point processes; they use the conventional dot-product score function to measure the similarity of two events while we introduce the more flexible score function based on neural networks which are learned from data. Another related work [21] leverages two individual attention structures to embed spatial and temporal information in order to predict traffic count, which differs from our setting, i.e., the discrete event modeling.

## II. ATLANTA TRAFFIC DATA-SET

In this section, we introduce a large-scale traffic dataset, which consists of three sub-datasets: (1) traffic congestion sub-dataset; (2) 911 call-for-service sub-dataset; and (3) traffic network sub-dataset.

### A. Traffic congestion

The traffic congestion data is a sub-dataset collected from the Georgia Department of Transportation (GDOT) [32], which records the real-time traffic condition on roads throughout the state of Georgia. These traffic data are recorded by traffic sensors installed on main traffic points in the highway system, where each sensor's data is organized as a series of numbers that indicate how many vehicles pass through the sensor every 5 minutes. The dataset also provides lane information at the locations where the sensors are installed. The number of lanes at the specific location of the highway allows us to estimate the maximum number of vehicles that the highway is able to process. We assume that the maximum number of vehicles that a highway can process is a linear function of the number of lanes.

Here, we consider 14 traffic sensors installed on two major highways (I-75 and I-85) in Atlanta shown in Figure 2, indexed by  $\mathcal{K} = \{1, 2, \dots, K\}$ ,  $K = 14$  and we denote their geo-locations (latitude and longitude) on the traffic network by  $r_k \in \mathcal{S} \subset \mathbb{R}^2, \forall k \in \mathcal{K}$ , where  $\mathcal{S}$  is the location space of the traffic network, which will be discussed in Section II-C. A traffic congestion event can be detected at certain time by a traffic sensor when the real-time traffic count exceeds the maximum number of vehicles that are allowed to pass through. Let  $\{x_i\}_{i=1}^{N_x(T)}$  represents a sequence of traffic congestion events in a single day, where  $N_x(T)$  is the number of the congestion events generated in the one-day horizon  $[0, T)$ . The  $i$ -th congestion event  $x_i = (t_i, s_i)$  is a data tuple consisting of the occurrence time  $t_i \in [0, T)$ , the sensor index  $s_i \in \mathcal{K}$ . We extracted 18,618 traffic congestion events for 174 days between April 2018 and December 2018 from the sub-dataset. The maximum and the minimum number of events in a single day is 168 and 19, respectively.

### B. 911 calls-for-service

As mentioned in Section I, traffic incidents may trigger unexpected congestion on the traffic network. We collected another sub-dataset from 911 calls-for-service reports of traffic incidents provided by the Atlanta Police Department (APD) [29], [33]. Such reports are generated by mobile patrol operations in the city, which handle 911 calls twenty-four hours a day. When a 911 call about a traffic incident comes in, a new incident record, including the *call time* and occurrence location, will be created at the dispatch center. Typically, after the new call arrives, the operator will assign an officer to handle the call. The unit arrives at the scene and starts the investigation. Once the police complete the investigation and clean the scene, the police report will be closed and record the *clear time*. The time interval that takes police to process the call between the call time and the clear time is called *processing time*. A 911 call with long processing time usually

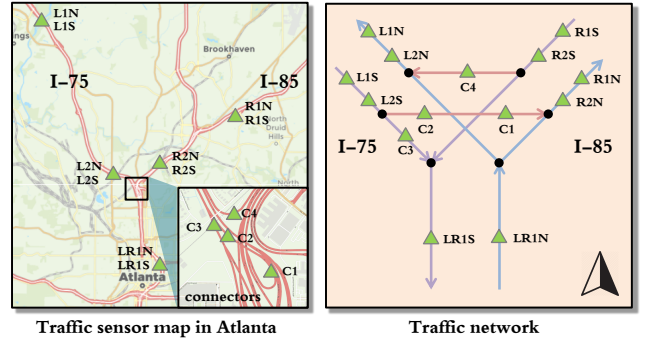


Fig. 2: The traffic network for major highways in Atlanta. **Left** shows the spatial distribution of traffic sensors, where green triangles represent locations of traffic sensors. Traffic sensors on the highway are bi-directional, i.e., two directions of the same location have separate traffic sensors to monitor the traffic condition. **Right** shows the traffic network and where traffic sensors located on the network. Each line segment represents one specific road segment, and black dots represent the confluence of two roads.

imposes a significant impact on the highway traffic condition where the 911 call is initiated.

Let  $\{y_j\}_{j=1}^{N_y}$  represent a sequence of traffic incidents reported by 911 calls in a single day, where  $N_y$  is the total number of the recorded 911-call incidents in one day. The  $j$ -th 911-call incident  $y_j = (t_j, r_j, z_j)$  is a data tuple consisting of the call time  $t_j \in [0, T)$ , the occurrence location  $r_j \in \mathcal{S}$  on the traffic network, and the processing time  $z_j \in \mathbb{R}_+$  indicating the length of time that the police takes to resolve the case. We select 19,805 such 911-call records that occurred on two major highways from the same period (between April 2018 and December 2018) with processing time larger than 15 minutes. Recorded 911-call incidents span over ten different categories, ranging from speeding tickets to massive car pileups.

### C. Traffic network

Due to the nature of traffic flow, there is a strong spatial dependence among the traffic data collected at different locations on the network. The network topology and the direction of the flow impose constraints on modeling such spatial correlations. For example, there should not be a correlation for data collected at two locations that do not share common traffic flow. In Downtown Atlanta, there are two major highways I-75/85 through the center of the city. These two highways start from the northwest and northeast side of the city, run due south, and meet each other in the Midtown, as shown in the left of Figure 2. Between I-75 and I-85, two connectors bridge two highways via single-direction ramps.

We extracted the network information of I-75 / I-85 and their connectors in Atlanta from OpenStreetMap [34], which is an editable map database and allows us to construct, visualize, and analyze complex traffic networks. The traffic network of a city is represented by a set of road segments defined in the OpenStreetMap dataset as shown in the right of Figure 2. Let  $\mathcal{S} \subset \mathbb{R}^2$  represents the set of all geo-locations on the network. We index road segments on the network by  $\mathcal{L} = \{1, \dots, L\}$ , where the set of locations on each segment is denoted as

$\mathcal{S}_l \subset \mathcal{S}, \forall l \in \mathcal{L}$ . For any location  $s \in \mathcal{S}$  on the network, we define the upstream portion  $\vee_s \subseteq \mathcal{S}$  of the network to include  $s$  itself and all locations upstream from  $s$ . We define the downstream portion  $\wedge_s \subseteq \mathcal{S}$  to include  $s$  itself and all locations downstream from  $s$ . For two locations  $u, v \in \mathcal{S}$ , the distance  $d(u, v) \in \mathbb{R}^+$  is defined as the stream distance along the highway if one of the two locations belongs to the downstream of the other. We denote  $u \rightarrow v$  when  $v$  belongs to  $\vee_u$  and the two points are said to be *flow-connected*. When two points are *flow-unconnected*, neither  $u$  belongs to  $\wedge_v$  nor  $v$  belongs to  $\wedge_u$ , and the relationship between  $u$  and  $v$  is denoted  $u \not\rightarrow v$ .

### III. METHODOLOGY

In this section, we propose an attention-based point process model for modeling traffic congestions and consider the police intervention for 911-call incidents as an exogenous promotion. The architecture of our model is shown in Figure 3.

#### A. Spatio-temporal point processes

Spatio-temporal point processes (STPPs) [2] consist of an ordered sequence of congestion events localized in time, location spaces. Let  $\{x_1, x_2, \dots, x_{N_x(T)}\}$  represents a sequence of congestion events sampled from a STPP and  $\{y_1, y_2, \dots, y_{N_y}\}$  represents a sequence of 911-call incidents recorded in the same time period. Recall that  $N_x(T)$  is the number of the congestion events generated in the time horizon  $[0, T)$  and  $N_y$  is the number of 911-call incidents. Let  $\mathcal{H}_t = \mathcal{X}_t \cup \mathcal{Y}_t$  denote the  $\sigma$ -algebra generated by all historical events before time  $t$ , where  $\mathcal{X}_t = \{x_i\}_{x_i < t}$ ,  $\mathcal{Y}_t = \{y_i\}_{y_i < t}$  denote the history of traffic congestions and the history of 911-call incidents, respectively. The congestions' distribution in STPPs are characterized via a conditional intensity function  $\lambda(t, k|\mathcal{H}_t)$ , which is the conditional probability of observing a traffic congestion at  $(t, k) \in [0, T) \times \mathcal{K}$  given the events' history  $\mathcal{H}_t$ .

Formally,  $\lambda(t, k|\mathcal{H}_t) = \mathbb{E}[N_k([t, t+dt)|\mathcal{H}_t]/dt]$ , where  $N_k(A)$  is the counting measure of events for sensor  $k$  over the set  $A \subseteq [0, T)$ .

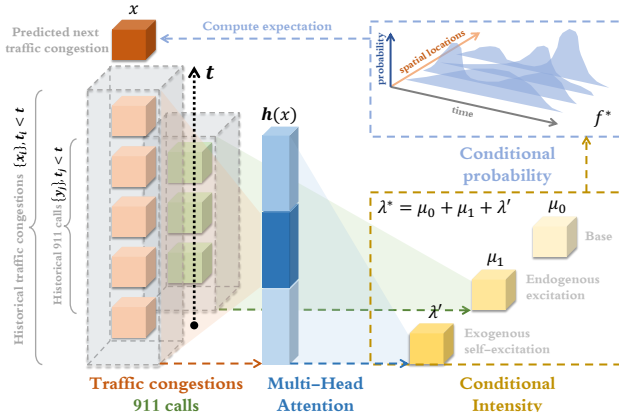


Fig. 3: The architecture for traffic congestion modeling.

To capture the dynamics between traffic congestions and 911-call incidents, we consider the following form for the conditional intensity function in our APP model:

$$\lambda(t, k|\mathcal{H}_t) = \underbrace{\mu_0(t, k)}_{\text{Background intensity}} + \underbrace{\mu_1(t, k|\mathcal{Y}_t)}_{\text{Exogenous promotion}} + \underbrace{\lambda'(t, k|\mathcal{X}_t)}_{\text{Endogenous self-excitation}}, \quad (1)$$

where  $\mu_0(t, k)$  is the background rate at  $(t, k)$ , which can be estimated from real data. The exogenous promotion  $\mu_1(t, k|\mathcal{Y}_t)$  captures the influence of past 911-call incidents reported by the police before time  $t$ . The endogenous self-excitation  $\lambda'(t, k|\mathcal{X}_t)$  captures the influence of past traffic congestions before time  $t$ . In the remainder of the section, we will discuss how to model these two types of excitations exactly in Section III-B and Section III-C, respectively.

#### B. Police intervention as exogenous promotion

As we discussed in Section II, the police intervention for 911-call incidents usually results in an increase in strain on urban traffic. This kind of strain only spreads along the traffic network and decays over the spatial correlation from where the 911-call incident originated. The spatial correlation between two locations  $u, v \in \mathcal{S}$  on the highway is determined by the structure of the traffic network and their stream distance  $d(u, v)$ . Also, the spatial correlation may vary from time to time since the traffic intensity is always changing throughout the day. Here, we denote such spatial correlation between two arbitrary locations  $u, v \in \mathcal{S}$  on the traffic network at time  $t \in [0, T)$  as  $\alpha_t(u, v) \in [0, 1]$ . We will discuss the estimation of such spatial correlation in Section III-E.

Now we consider the police intervention of the 911-call incident  $y_j = (t_j, r_j, z_j)$  at  $(t, k)$  as an additive exogenous promotion when  $t$  is in the middle of process of the event  $y_j$ , i.e.,  $t \in [t_j, t_j + z_j)$ . Formally, the exogenous promotion can be defined as

$$\mu_1(t, k|\mathcal{Y}_t) = \sum_{y_j \in \mathcal{Y}_t} \gamma \alpha_t(r_k, r_j) \cdot \delta_t([t_j, t_j + z_j)) \quad (2)$$

where  $\delta_t(A)$  is the Dirac measure, i.e., taking the value 1 when  $t \in A$  and 0 otherwise. The  $\gamma$  is the parameter that captures the decay rate of the influence over their spatial correlation  $\alpha_t(r_k, r_j)$ .

#### C. Attention-based self-excitation modeling

The idea of Attention-based Point Processes (APP) is to model the nonlinear dependence of the current traffic congestion event from past congestion events using the attention mechanism [11], [12]. Specifically, we model the endogenous self-excitation  $\lambda'(t, k|\mathcal{X}_t)$  in (1) using the output of the attention structure. We also consider multi-heads in the attention mechanism [12], which offers multiple “representation subspace” for events in the sequence. The exact calculation of the conditional intensity is carried out as follows.

For notational simplicity, let  $x_n := (t_n, s_n)$  represent the data tuple of the current congestion event and  $x_i := (t_i, s_i) \in \mathcal{X}_{t_n}$  represent the data tuple of the  $i$ -th event in the past. As shown in Figure 4, for the  $m$ -th attention head, we score the current congestion event against its past event, denoted



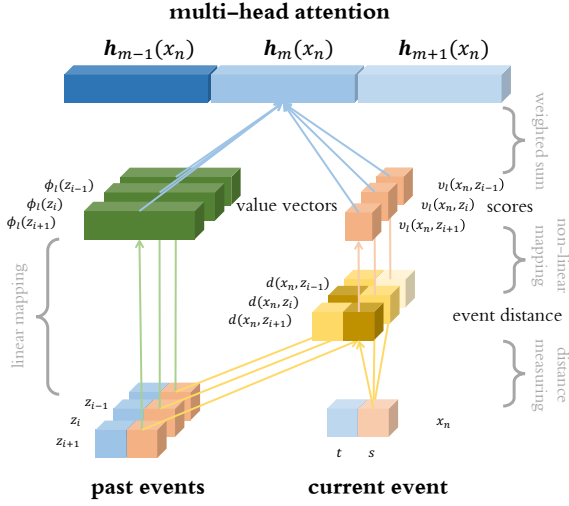


Fig. 4: The multi-head attention architecture.

as  $v_m(x_n, x_i) \in \mathbb{R}^+$ . For the event  $x_n$ , the score  $v_m(x_n, x_i)$  determines how much *attention* to place on the past event  $x_i$  as we encode the history information, which will be further discussed in Section III-D. The normalized score  $\tilde{v}_m(x_n, x_i) \in [0, 1]$  for the event  $x_n$  and  $x_i$  is obtained by employing the softmax function over the score, which is defined as:

$$\tilde{v}_m(x_n, x_i) = \frac{v_m(x_n, x_i)}{\sum_{x_j \in \mathcal{X}_{t_n}} v_m(x_n, x_j)}, \quad (3)$$

Then we are able to obtain the  $m$ -th attention head  $\mathbf{h}_m(x_n) \in \mathbb{R}^p$  for the event  $x_n$  via multiplying each value embedding by the score and adding them up, which is formally defined as

$$\mathbf{h}_m(x_n) = \sum_{x_i \in \mathcal{X}_{t_n}} \tilde{v}_m(x_n, x_i) \phi_m(x_i), \quad (4)$$

where the value embedding  $\phi_m(x) = x^\top W_m^v$  and  $W_m^v \in \mathbb{R}^{d \times p}$  is a weight matrix, the  $d$  is the data dimension (here,  $d = 3$ ) and  $p$  is the dimension of value embedding. In contrast to the *self-attention* mechanism [12], the current event  $x_n$  and past event  $x_i$  are analogous to *query* and *key*, respectively. The value embedding for the past event  $\phi_m(x_i)$  is analogous to *value*. The multi-head attention  $\mathbf{h}(x) \in \mathbb{R}^{M \times p}$  for event  $x$  is the concatenation of  $M$  single attention heads:

$$\mathbf{h}(x) = \text{concat}(\mathbf{h}_1(x), \dots, \mathbf{h}_M(x)).$$

Now, let  $x := (t, k)$  represent the congestion event at  $(t, k)$  and denote  $\lambda'(t, k | \mathcal{X}_t)$  in (1) as  $\lambda'(x | \mathcal{X}_t)$ . The historical information in  $\mathcal{X}_t$  can be modeled as a non-linear transformation of the multi-head attention  $\mathbf{h}(x)$ . Hence, the endogenous self-excitation  $\lambda'$  can be specified as:

$$\lambda'(x | \mathcal{X}_t) = \lambda'(x | \mathbf{h}(x)) = \text{softplus}(\mathbf{h}(x)^\top W + b), \quad (5)$$

where  $W \in \mathbb{R}^{L \times p}$ ,  $b \in \mathbb{R}$  are the weight matrix and the bias term. The function  $\text{softplus}(x) = \log(1 + e^x) > 0$  is a smooth approximation of the ReLU function, which ensures the intensity strictly positive at all times when an event could possibly occur and avoid infinitely bad log-likelihood.

#### D. Score function

The score function directly quantifies how likely one event is to be triggered by another event in history. The dot-product score function has been widely used in most of the attention models. Typically, the score is obtained by computing the inner product between query  $x_n$  and key  $x_i$ , i.e.,  $v(x_n, x_i) = x_n^\top x_i$ , which is their Euclidean distance in the embedding space. However, as discussed in Section III-B, for the traffic application, the correlation of two locations on the highway may not depend on their Euclidean distance exactly, and this correlation may also vary over time. Again, we adopt the spatial correlation  $\alpha_t(r_{s_n}, r_{s_i})$  at time  $t$  between locations of two events  $r_{s_n}, r_{s_i} \in \mathcal{S}$  rather than their Euclidean distance. The estimation of the spatial correlation will be discussed in Section III-E.

As shown in Figure 5, the score  $v_m(x_n, x_i)$  for the  $m$ -th attention head can be expressed as:

$$v_m(x_n, x_i) = \psi_{\theta_m}(t_n - t_i, \alpha_{t_n}(r_{s_n}, r_{s_i})), \quad (6)$$

where the  $\psi_{\theta_m}(\cdot, \cdot) \in \mathbb{R}^+$  is a multi-layer neural network parameterized by a set of weights and biases denoted by  $\theta_m$ . The neural network takes the spatial correlation  $\alpha_{t_n}(r_{s_n}, r_{s_i})$  and the temporal distance  $t_n - t_i$  as input and yields a non-negative score. The score function can be interpreted as a weighted spatio-temporal distance, where the weights of time and space are learned from the data. Note that the score function for each attention head may be different.

#### E. Tail-up spatial model in score function

To capture the spatial correlation  $\alpha_t(u, v)$  between two locations  $u, v \in \mathcal{S}$  on the traffic network at time  $t \in [0, T)$ , we adopt the tail-up spatial model, which is originally proposed based on moving average constructions in [35], [36], [37], [38] and widely used in the river network modeling [39], [40], [41]. For notational simplicity, we omit  $t$  in the following of this section. There are three major advantages of tail-up models

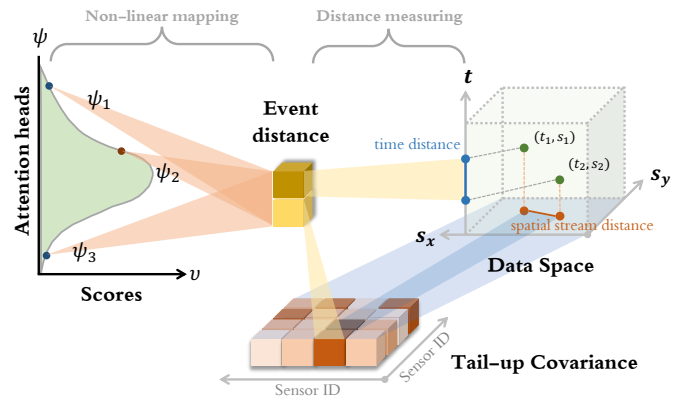


Fig. 5: The illustration for the score calculation. First, we measure the distance between two events, where their spatial correlation is represented by our tail-up model; then, we calculate the score by transforming their distance via a non-linear mapping. Note that we use different non-linear mapping for different attention head.

against other methods. (1) The tail-up models use stream distance rather than the Euclidean distance, which is defined as the shortest distance along with the stream network between two locations. (2) The statistical independence is imposed on the observations located on stream segments that do not share traffic flow. (3) Proper weighting is incorporated on the entries of the covariance matrix when the road segments in the network are splitting into multiple segments to ensure that the resulting covariance is stationary. The tail-up models are especially appropriate when we want to enforce zero covariance when locations are flow-unconnected. This situation can occur when the flow dominates a variable (e.g., when traffic congestion enters a stream and can only move upstream, it will cause measurements to be autocorrelated only when flow-connected).

The traffic at location  $u \in \mathcal{S}$  can be viewed as a white-noise random process  $Z_u$ , where observable locations on the traffic network can be developed by creating random variables as the integration of a moving average function over the process on the upstream of the network [40],

$$Z_u = \mu_u + \int_{\mathcal{V}_u} g(r-u) \sqrt{\frac{w(r)}{w(u)}} dB(r),$$

where  $\mu_u$  is a deterministic mean process at location  $u$ ,  $\mathcal{V}_u$  notes the upstream of location  $u$  and  $w(r) = w^l$  for all location  $r \in \mathcal{S}_l$  on the segment  $l$ , which is the weight that check an additivity constraint to ensure stationarity in variance. The weights can be estimated using normalized average traffic counts for each segment on the traffic network. Moving average function  $g(\cdot)$  is square-integrable and defined on  $\mathbb{R}$ . The  $B(r), r \in \mathcal{S}$  is a Brownian process starting from sources of the traffic network, progressing toward outlets, and separating or merging themselves in Brownian processes at traffic forks. The spatial correlation  $\alpha(u, v)$  is obtained by  $\text{cov}(Z_u, Z_v) = \mathbb{E}[Z_u Z_v] - \mathbb{E}[Z_u] \mathbb{E}[Z_v]$ , i.e.,

$$\alpha(u, v) = \int_{\mathcal{V}_u \cap \mathcal{V}_v} g(s-u) g(s-v) \frac{w(s)}{\sqrt{w(u)w(v)}} ds.$$

Let  $\Delta r$  be a stream distance on  $\mathbb{R}^+$  and define  $C(\Delta r) := \int_{\mathbb{R}} g(r) g(r - \Delta r) dr$ . By choosing particular moving average functions, we are able to reparameterize  $C(\cdot)$  and put the model in forms typically seen in the spatial statistical literature. We adopt the tail-up exponential model here [38], i.e.,

$$C(\Delta r) := \beta \exp(-\Delta r / \sigma),$$

where  $\beta, \sigma$  are the parameters of the tail-up model. Let  $d(u, v) \in \mathbb{R}^+$  be the stream distance between locations  $u, v \in \mathcal{S}$  on the traffic network. The above covariance can be simplified as:

$$\alpha(u, v) = \begin{cases} C(d(u, v)) \sqrt{\frac{w(u)}{w(v)}}, & u \rightarrow v \\ 0, & u \not\rightarrow v. \end{cases} \quad (7)$$

which defines the support of  $\alpha(u, v)$ .

For example in Figure 6, we first define all weights for each segment, i.e.,  $\{w^l\}_{l=1}^L$ . The structure of the traffic network ensures that the sum of weights that flow into a confluence equals to the sum of weights that flow out of the same

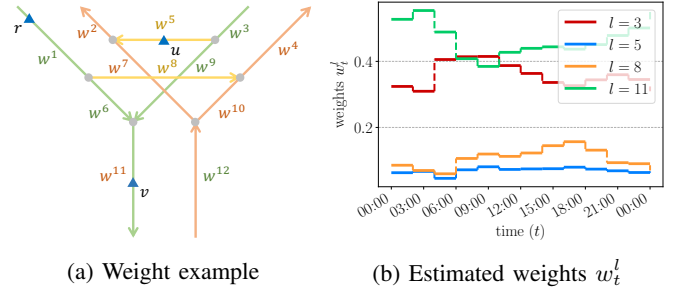


Fig. 6: Weighting example for the tail-up model: arrows indicate flow directions of segments on the traffic network; gray dots represent confluences;  $w_i$  is the weight of the segment  $i$ ; triangle  $u, v$ , and  $r$  are observable locations.

confluence (e.g.  $w^1 = w^6 + w^7$  and  $w^6 + w^9 = w^{11}$ ). Then we can obtain  $\alpha(u, r) = C(d(u, v)) \sqrt{w(u)/w(v)} = C(d(u, v)) \sqrt{w^5/w^{11}}$  and  $\alpha(u, r) = 0$  because location  $u$  and  $r$  are flow-unconnected.

In the experiment, we consider the tail-up model to be time-variant, i.e., for each time  $t$ , we can obtain a set of weights  $\{w_t^l\}_{l \in \mathcal{L}}$  and spatial correlation  $\alpha_t(u, v)$  by estimating the traffic counts at time  $t$ , since the distribution of the traffic flow may vary over time. For example, as shown in Figure 6 (b), the time-variant weights of four traffic sensors are estimated based on the normalized traffic counts for every two hours.

#### F. Online attention for streaming data

For streaming data, the attention calculation may be computationally intractable since past events would explode in number as time goes on. Here, we propose an adaptive online attention algorithm to address this issue. Only a fixed number of ‘‘important’’ historical events with high average scores will be remembered for the attention calculation in each attention head. In both synthetic and real datasets, we have shown that, in some cases, only very few events could impose a dominant influence on their future events. Our APP model can be performed efficiently via the online algorithm using a small portion of historical data,

The procedure for collecting ‘‘important’’ events in each attention head is demonstrated as follows: first, when the  $n$ -th event occurs, for a past event  $x_j, t_j < t_n$  in  $m$ -th attention, we denote the set of its score against the future congestion events  $\{\tilde{v}_m(x_n, x_j)\}_{n: t_j \leq t_n}$  as  $\mathcal{C}_{j,m}$ ; then the average score of the event  $x_j$  can be computed by  $\mu_{j,m} = (\sum_{s \in \mathcal{C}_{j,m}} s) / |\mathcal{C}_{j,m}|$ , where  $|A|$  denotes the number of elements in set  $A$ . Hence, a recursive definition of the set  $\mathcal{A}_{n,m}$  for selected events in the  $m$ -th attention head up until the occurrence of the event  $x_n$  is written as:

$$\begin{aligned} \mathcal{A}_{n,m} &= \mathcal{X}_{t_{n+1}}, & \forall n \leq \eta, \\ \mathcal{A}_{n,m} &= \mathcal{A}_{n-1,m} \cup \arg \max_{z_j: t_j < t_n} \{\mu_{j,m}\} \setminus \arg \min_{z_j: t_j < t_n} \{\mu_{j,m}\}, & \forall n > \eta, \end{aligned}$$

where  $\eta$  is the maximum number of events we will retain. The exact event selection is carried out by Algorithm 1. To perform the online attention, we substitute  $\mathcal{X}_{t_n}$  in (6) and (4) with  $\mathcal{A}_{n,m}$  for all attention heads.

---

**Algorithm 1** Event Selection for Online Attention
 

---

**Input:** data  $\mathbf{x} = \{x_i\}_{i=1}^{n-1}$  and  $x_n$ , threshold  $\eta$ .  
 Initialize  $\mathcal{A}_{0,m} = \emptyset$ .  
**for**  $n = 1$  **to**  $+\infty$ . **do**  
   **for**  $m = 1$  **to**  $M$ . **do**  
      $\mathcal{A}_{n,m} \leftarrow \mathcal{A}_{n-1,m} \cup x_n$ .  
     Initialize  $\mathcal{C}_{n,m} = \emptyset$ ,  $\mu_{j,m} = 0$ .  
     **for**  $j = 1$  **to**  $n - 1$  **do**  
        $\mathcal{C}_{j,m} \leftarrow \mathcal{C}_{j,m} \cup \tilde{v}_m(x_n, x_j)$ .  
        $\mu_{j,m} \leftarrow (\sum_{s \in \mathcal{C}_{j,m}} s) / |\mathcal{C}_{j,m}|$ .  
     **end for**  
     **if**  $i > \eta$  **then**  
        $\mathcal{A}_{n,m} \leftarrow \mathcal{A}_{n-1,m} \setminus \arg \min_{z_j: t_j < t_n} \{\mu_{j,m}\}$ .  
     **end if**  
   **end for**  
**end for**

---

### G. Learning and Inference

The model is jointly parameterized by a set of parameters  $\{W, b, \gamma, \beta, \sigma, \{\theta_m, W_m^v\}_{m=1}^M\}$ . We fit the model by maximum likelihood, which can be solved by stochastic gradient descent. Equipped with the definition of conditional intensity in (1), we can write down the likelihood function explicitly. Suppose there are a total of  $n$  samples before the time horizon  $T$  denoted as  $\mathbf{x} = \{(t_i, s_i)\}_{i=1}^{N_x(T)}$ . Let  $F^*(t, k) = \mathbb{P}\{t_{n+1} < t, k | \mathcal{H}_t\}$  be the conditional probability that next congestion event  $(t_{n+1}, k)$  happens before  $t$  given the history of the previous events and let  $f^*(t, k)$  be the corresponding conditional density probability. To avoid the notational overload, we denote the conditional intensity function  $\lambda(t, k | \mathcal{H}_t)$  as  $\lambda^*(t, k)$ . The conditional intensity function for arbitrary sensor  $k$  is defined by  $\lambda^*(t, k) = f^*(t, k) / (1 - F^*(t, k))$ . From the definition above, we can show  $\lambda^*(t, k) = -d \log(1 - F^*(t, k)) / dt$  and hence,  $\int_{t_n}^t \lambda^*(\tau, k) d\tau = -\log(1 - F^*(t, k))$ , where  $F^*(t, k) = 0$ , since the  $(n+1)$ -th event does not exist at time  $t_n$ . Therefore,  $F^*(t, k) = 1 - \exp\{-\int_{t_n}^t \lambda^*(\tau, k) d\tau\}$  and

$$f^*(t, k) = \lambda^*(t, k) \cdot \exp\{-\int_{t_n}^t \lambda^*(\tau, k) d\tau\}. \quad (8)$$

Then the log-likelihood of observing the sequence  $\mathbf{x}$  can be obtained by:

$$\ell(\mathbf{x}) = \sum_{i=1}^{N_x(T)} \log \lambda^*(t_i, s_i) - \sum_{k \in \mathcal{K}} \int_0^T \lambda^*(t, k) dt. \quad (9)$$

To perform the event prediction given a sequence of events  $\{x_i\}_{i=1, \dots, n}$  with length of  $n$ , we estimate the next event  $(\hat{t}_{n+1}, \hat{s}_{n+1})$  by calculating the expectation of the conditional probability defined in (8):

$$\begin{bmatrix} \hat{t}_{n+1} \\ \hat{s}_{n+1} \end{bmatrix} = \begin{bmatrix} \int_{t_n}^T \tau \sum_{k \in \mathcal{K}} f^*(\tau, k) d\tau \\ \arg \max_{k \in \mathcal{K}} \int_{t_n}^T f^*(\tau, k) d\tau \end{bmatrix}. \quad (10)$$

In general, the integration above cannot be obtained analytically. Therefore, we use common numerical integration techniques here to compute the expectation.

## IV. EXPERIMENTAL RESULTS

In this section, we first conduct experiments on four synthetic datasets to illustrate our attention-based point process model's effectiveness. Then we test our model on the large-scale Atlanta traffic dataset. We evaluate our model with/without the online attention (APP / OAPP) and other baseline methods by comparing their log-likelihood and visually inspecting their conditional intensity function in both temporal and spatial scenarios. There are five baseline methods that we are considering in the following experiments:

**Long-Short Term Memory (LSTM)** is a specialized recurrent neural network (RNN) used for sequential data modeling. Here, we feed the event series into the LSTM and obtain the hidden state as a summary of the historical information. Then the LSTM can generate the next event via an output layer given the last hidden state.

**Recurrent Marked Temporal Point Process (RMTPP)**: [3] assumes the following form for the conditional intensity function  $\lambda^*$  in point processes, denoted as  $\lambda^*(t) = \exp(\mathbf{v}^\top \mathbf{h}_j + \omega(t - t_j) + b)$ , where the  $j$ -th hidden state in the RNN  $\mathbf{h}_j$  is used to represent the history influence up to the nearest happened event  $j$ , and  $w(t - t_j)$  represents the current influence. The  $\mathbf{v}, \omega, b$  are trainable parameters.

**Neural Hawkes Process (NHP)**: [4] specifies the conditional intensity function in temporal point processes using a continuous-time long-short term memory (LSTM), denoted as  $\lambda^*(t) = f(\omega^\top \mathbf{h}_t)$ , where the hidden state of the LSTM up to time  $t$  represents the history influence, the  $f(\cdot)$  is a softplus function which ensure the positive output given any input.

**Self-Attentive Hawkes Process (SAHP)**: [31] adopts self-attention mechanism to model the historical information in the conditional intensity function, which is specified as  $\lambda^*(t) = \text{softmax}(\mu + \alpha \exp\{\omega(t - t_j)\})$ , where  $\mu, \alpha, w$  are computed via three non-linear mappings:  $\mu = \text{softplus}(\mathbf{h}W_\mu)$ ,  $\alpha = \tanh(\mathbf{h}W_\alpha)$ ,  $\omega = \text{softplus}(\mathbf{h}W_\omega)$ . The  $W_\mu, W_\alpha, W_\omega$  are trainable parameters.

**Hawkes Process (HP)**: [26] as one of the state-of-the-art in temporal events modeling, the conditional intensity function of Hawkes process is given by  $\lambda^*(t) = \mu + \alpha \sum_{t_j < t} \beta \exp\{-\beta(t - t_j)\}$ , where parameters  $\mu, \alpha, \beta$  can be estimated via maximizing likelihood.

The experiment configurations are as follows. A three-layer neural network in (6) and three attention heads in (5) are employed for our model. Note that using multiple layers in neural networks and multiple numbers of heads are critical to our final experimental results. Each dataset is divided into 80% training and 20% testing data. For training, the model parameters are estimated using the training data. For optimization, we employ Adam optimizer with a learning rate =  $10^{-3}$  while the batch size is 64. The objective is to minimize the negative log-likelihood function derived in (9). For testing, both estimated intensity and log-likelihood are evaluated. Moreover, for OAPP, only 50% number of events are retained for training, i.e.,  $\eta = 0.5n$ ,  $n$  is the maximum length of sequences in the dataset.

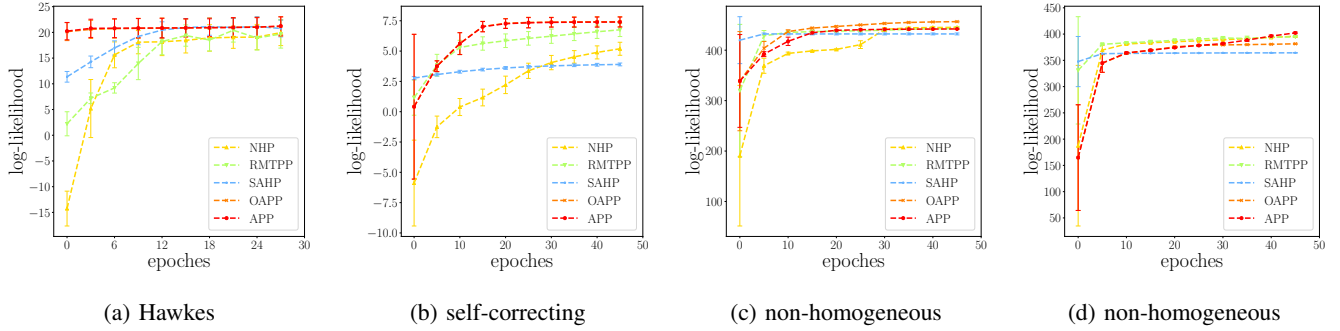


Fig. 7: The average log-likelihood of synthetic datasets versus training epochs. For each synthetic dataset, we evaluate the performance of the five methods based on the maximum log-likelihood averaged per series calculated for the test data.

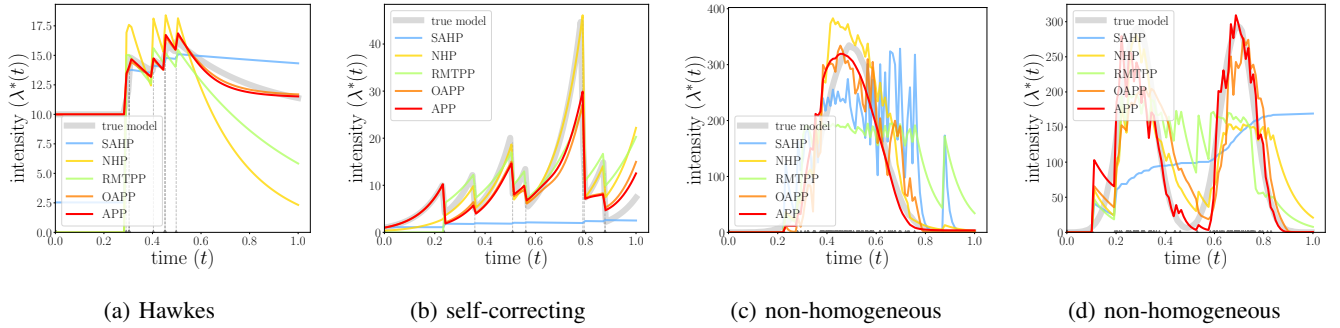


Fig. 8: The conditional intensity function estimated from synthetic datasets. Triangles at the bottom of each panel represent events. The ground truth of conditional intensities is indicated by the grayline.

TABLE I: Average maximum log-likelihood on synthetic data.

| DATA SET        | SAHP  | NHP   | RMTTP | APP          | OAPP         |
|-----------------|-------|-------|-------|--------------|--------------|
| HAWKES          | 20.8  | 20.0  | 19.7  | <b>21.2</b>  | 21.1         |
| SELF-CORRECTION | 3.5   | 5.4   | 6.9   | 7.1          | <b>7.1</b>   |
| NON-HOMO 1      | 432.4 | 445.6 | 443.1 | 442.3        | <b>457.0</b> |
| NON-HOMO 2      | 364.3 | 410.1 | 405.1 | <b>428.3</b> | 420.1        |

### A. Synthetic data

To compare conditional intensities generated by various of approaches in a more intuitive way, we first consider time series data, where each data point is a one-dimensional timestamp. To adapt our APP model to time-only scenarios, we only consider the temporal distance in the score function of APP. i.e., substitute (3) with  $v_m(x_n, x_i) = \psi_{\theta_m}(t_n - t_i)$ .

In the following experiments with synthetic time series data, we confirmed that our APP is capable of capturing the temporal pattern of synthetic data generated from conventional generative processes. To quantitatively evaluate each method's performance, we first measure the average maximum likelihood of the models on each synthetic dataset. We know the true intensities of these generating processes. We also plot the conditional intensity function over time given one particular event series, and visually inspect whether the trained models accurately predict these intensities.

The synthetic data are obtained by the following four generative processes: (1) *Hawkes process*: the conditional intensity function is given by  $\lambda^*(t) = \mu + \alpha \sum_{t_j < t} \beta \exp(-\beta(t - t_j))$ , where  $\mu = 10$ ,  $\alpha = 1$ , and  $\beta = 1$ ; (2) *self-correction point process*: the conditional intensity function is given by

$\lambda^*(t) = \exp(\mu t - \sum_{t_i < t} \alpha)$ , where  $\mu = 10$ ,  $\alpha = 1$ ; (3) *non-homogeneous Poisson 1*: The intensity function is given by  $\lambda^*(t) = c \cdot \Phi(t - 0.5) \cdot U[0, 1]$  where  $c = 100$  is the sample size, the  $\Phi(\cdot)$  is the PDF of standard normal distribution, and  $U[a, b]$  is uniform distribution between  $a$  and  $b$ ; (4) *non-homogeneous Poisson 2*: The intensity function is a composition of two normal functions, where  $\lambda^*(t) = c_1 \cdot \Phi(6(t - 0.35)) \cdot U[0, 1] + c_2 \cdot \Phi(6(t - 0.75)) \cdot U[0, 1]$ , where  $c_1 = 50$ ,  $c_2 = 50$ . Each synthetic dataset contains 5,000 sequences with an average length of 30, where each data point in the sequence only contains the occurrence time of the event.

Figure 7 summarizes the log-likelihood value of each model versus the training epochs, where each epoch includes 125 batches, and each batch randomly takes 40 sequences as training data. The higher log-likelihood value indicates better performance the model achieves. As we can see from Figure 7 and Table I, our APP outperforms other four baseline methods on all four synthetic datasets with the largest average maximum log-likelihood value. Besides, our OAPP also shows competitive performances, where only 50% of events are used in online attention calculation.

Figure 8 shows the estimated intensities using different methods in contrast to the true latent intensities indicated by the gray lines. We compare the predictive performance of the proposed model fitted to three types of time series models. Our APP can better capture the true conditional intensity function for all four synthetic datasets compared to the other four baseline methods.



TABLE II: Average maximum log-likelihood and prediction accuracy using Atlanta traffic dataset.

| MODELS          | $\max \ell$<br>(TIME ONLY) | $\max \ell$<br>(TIME & SPACE) | PREDICTION<br>ACCURACY |
|-----------------|----------------------------|-------------------------------|------------------------|
| LSTM            | N/A                        | N/A                           | 18.5%                  |
| HP              | 339.9                      | 307.5                         | 8.82%                  |
| RMTPP           | 339.2                      | 490.1                         | 22.0%                  |
| NHP             | 324.4                      | N/A                           | N/A                    |
| SAHP            | 326.7                      | N/A                           | N/A                    |
| APP + EUCLIDEAN | 392.3                      | 570.7                         | 30.9%                  |
| APP + TAILUP    | <b>458.5</b>               | <b>636.2</b>                  | <b>37.6%</b>           |
| OAPP + TAILUP   | 437.5                      | 615.9                         | 36.9%                  |

### B. Traffic data

In this section, we further illustrate the effectiveness of our model by experimenting on the Atlanta traffic dataset. In addition to time, we also consider spatial information in our APP. Apart from comparisons between other spatio-temporal based baseline approaches, we also compare our model using the tail-up spatial correlation defined in (7) (APP+Tailup) and using Euclidean distance (APP) as a sanity check. The model can be evaluated quantitatively by computing their maximum log-likelihood and prediction accuracy using (10). Also, we evaluate and visually inspect the conditional intensity for each traffic sensor over time. Last but not least, we will also provide an intuitive interpretation for the score and tail-up spatial correlation obtained from the fitted APP model.

As shown in Figure 9, we compare and report the average log-likelihood for each method over training epochs. The results show that our method outperforms other baseline methods by attaining the largest log-likelihood for both time-only and space-time traffic datasets when the model achieves its convergence. We also summarize the maximum log-likelihood for each method with or without spatial information in Table II and their prediction accuracy<sup>1</sup>, in which our method attains the best performance regarding both two metrics.

We also evaluate the conditional intensity of each traffic sensor using the fitted APP for traffic datasets. As discussed in Section I, there are 14 traffic sensors installed along two major highways (I-75 and I-85) in Atlanta, as shown in the left of Figure 11. For better presenting the spatial pattern captured by the mode, we select two typical days in Atlanta, i.e., May 8th, 2018, and April 24th, 2018.

Figure 11 (a) shows a clear temporal pattern on a regular weekday (Tuesday, May 8th, 2018), where the intensity of each sensor reaches its pinnacle in both mornings (around 7:00) and evening (around 16:00) rush hours; Figure 11 (b) shows the intensities on another weekday (Tuesday, April 24th, 2018). On this day, Atlanta broke a 135-year-old rainfall record when it got 4.16 inches of rain [42]. The previous record, set in 1883, was 2.4 inches. As we can see from the figure, the heavy rain and subsequent flood in the city led to an unusual level of traffic congestion. Differing from the results shown in Figure 11 (a), the traffic congestion level remains at a relatively high level throughout the entire day.

We also categorize the traffic sensors into three sub-groups based on their locations and plot their conditional intensities

<sup>1</sup>The prediction accuracy, if using random guess, is 7.1% since there are 14 sensors

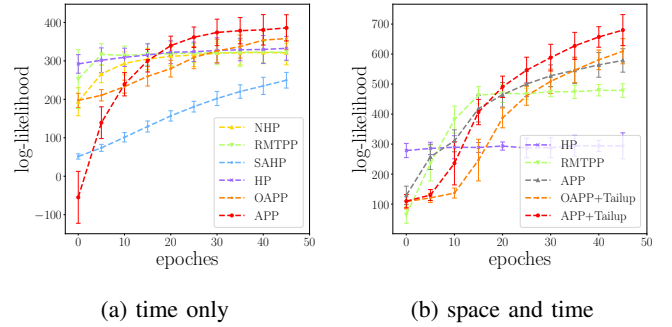


Fig. 9: The average log-likelihood of Atlanta traffic data versus training epochs with and without considering spatial information.

individually shown at the bottom of each subplot. It has been shown that similar temporal patterns can be found among the traffic sensors in the same sub-group since these sensors are installed along the same direction of the road and sharing the same traffic flow. Moreover, there exists a “phantom traffic jam” phenomenon [43] according to the above results. This kind of situation usually begins when a part of traffic flow slows down even slightly, then causes the flow behind that part to slow even more, and the slowing action spreads backward through the lane of traffic like a wave, getting worse the farther it spreads. For example, as the sensor  $L1S$ ,  $L2S$ ,  $LR1S$  are distributed along the southbound of I-75, the peak of intensity of the first sensor appears later about half an hour against the following sensors. The congestion can clog up the road, and the traffic wave would drift downward when the first congestion occurs. Similar phenomenons can also be found among the sensor  $L1N$ ,  $L2N$ ,  $LR1N$ .

**Score function interpretation.** To interpret the result of our score function, we visualize the scores of current event  $x_n$  against its historical events  $\{z_i\}_{i=1}^{n-1}$  in Figure 10, where the first 15 events in a row in a sequence are considered. Specifically, the entry at the  $n$ -th row and the  $i$ -th column of

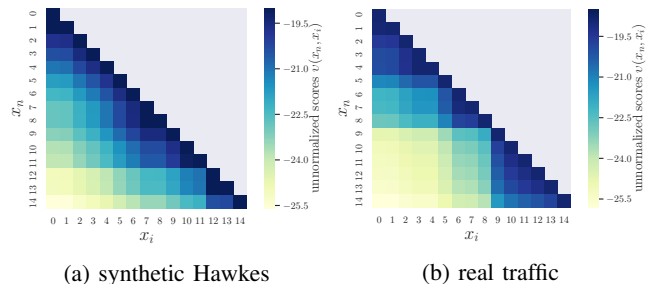


Fig. 10: Visualization of scores (discussed in Section III-D) between pairwise events in the sequence, learned from data using (a) synthetic data generated from a Hawkes process model and (b) traffic data collected from the GDOT. The  $x_n$  represents the current event and  $x_i$  represents past events, where  $t_i < t_n$ . The color of the entry at the  $n$ -th row and the  $i$ -th column represents the score  $v(x_n, x_i)$  learned from data using our DAPP model.

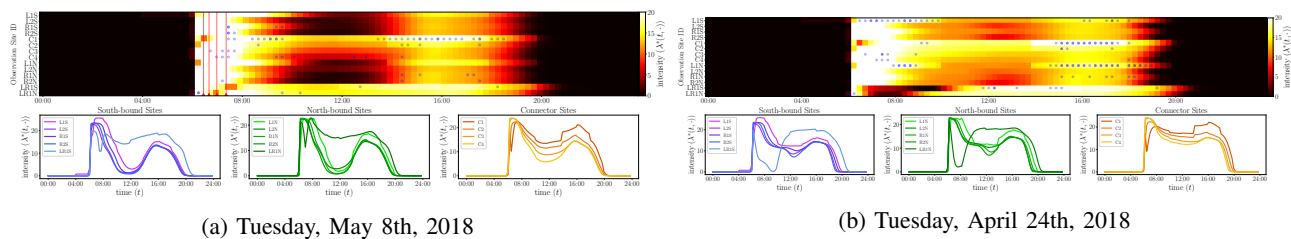


Fig. 11: (a) The heatmap shows the conditional intensities of 14 traffic sensors in a single day. Each row represents a traffic sensor (associated with a unique site ID), each column representing a particular time slot, blue dots represent the occurrence of events, and red vertical lines represent 911 calls. The color depth in the heatmap represents the level of intensity. (b) We categorize the conditional intensity into three subplots, where three plots from left to right represent the intensity of five sites on northbound highways, five sites on southbound highways, and four sites on connectors, respectively.

the lower triangular matrix represents scores of the event  $x_n$  against its past event  $x_i$ , i.e.,  $v(x_n, x_i)$ .

As shown in Figure 10, our APP can capture the complex dependence between events accurately. In particular, Figure 10 (a) shows the scores of events generated from a Hawkes process defined in Section IV-A. The pattern of scores for events against their past resembles the exponential decay, which is defined in the kernel function. We also conduct a similar experiment on the traffic dataset, as shown in Figure 10 (b). There is a community structure, where the first nine events pose a much weaker impact on their subsequent events than others, i.e., the first nine scores in the last row are remarkably lower than the other scores. By investigating the data, we find out that the first nine events are observed by the traffic sensor installed on the northbound of the highway. In contrast, others are observed by other sensors installed in the opposite direction, i.e., these two sets of traffic sensors are flow-unconnected, which meets the community structure we observed in the score matrix shown in Figure 10 (b).

**Tail-up spatial correlation interpretation.** The spatial correlation between 14 traffic sensors learned by our tail-up model is highly interpretable. As shown in Figure 12, we visualize three covariance matrices of 14 traffic sensors corresponding to three different periods: morning rush hour, evening rush hour, and the midnight. As we can see from the spatial structure of these covariance matrices. (1) There are two community structures among two sets of traffic sensors, which correspond to locations on the southbound and the northbound of highways, respectively. (2) The covariance between the highway connectors ( $C1-C4$ ) and the southbound of highways ( $L1S, L2S, R1S, R2S$ ) are sensitive to the rush hour. These two observations confirm the idea that the triggering effect between congestion events could be spatially structured and directional. The highway connectors, in particular, play a vital role in this mechanism.

## V. CONCLUSION

We develop a novel attention-based point process model for modeling the dynamics of traffic congestion with consideration of the influence of 911-call incidents reported by the police. The goal is to model traffic congestion events and the triggering effect while taking advantage of traffic networks' structural knowledge.

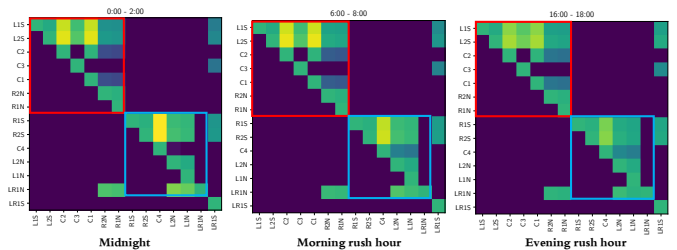


Fig. 12: Comparison of spatial correlation between 14 traffic sensors generated by the tail-up model. The red and blue boxes indicate the correlations between traffic sensors located in southbound and northbound of highways, respectively.

As demonstrated by our experiments, our method achieves the best performance in maximizing the likelihood of a point process compared with previous approaches as well as prediction accuracy on the traffic dataset. Besides, by implementing various kinds of point process models, we show that our model exceeds the others in terms of robustness and flexibility. Furthermore, based on the structural information of dynamic networks, our model can be generalized so that predicting the current event of a particular type might depend more on specific types of events by exploring the structure of the score matrices. This gives us a new method for implementing causality inference in networks.

## REFERENCES

- [1] D. Wickert, "Is there a fix for i-85 traffic?" <https://www.ajc.com/news/transportation/there-fix-for-traffic/FBjOFLgKw7kGphc3itpvvJ/>, Feb 2020.
- [2] A. Reinhardt, "A review of self-exciting spatio-temporal point processes and their applications," 2017.
- [3] N. Du, H. Dai, R. Trivedi, U. Upadhyay, M. Gomez-Rodriguez, and L. Song, "Recurrent marked temporal point processes: Embedding event history to vector," in *Proceedings of the 22nd ACM SIGKDD International Conference on Knowledge Discovery and Data Mining*, ser. KDD '16. New York, NY, USA: Association for Computing Machinery, 2016, pp. 1555–1564.
- [4] H. Mei and J. M. Eisner, "The neural Hawkes process: A neurally self-modulating multivariate point process," in *Advances in Neural Information Processing Systems 30*. Curran Associates, Inc., 2017, pp. 6754–6764.
- [5] S. Li, S. Xiao, S. Zhu, N. Du, Y. Xie, and L. Song, "Learning temporal point processes via reinforcement learning," in *Proceedings of the 32nd International Conference on Neural Information Processing Systems*, ser. NIPS '18. Red Hook, NY, USA: Curran Associates Inc., 2018, pp. 10 804–10 814.

- [6] U. Upadhyay, A. De, and M. Gomez Rodriguez, "Deep reinforcement learning of marked temporal point processes," in *Advances in Neural Information Processing Systems 31*, S. Bengio, H. Wallach, H. Larochelle, K. Grauman, N. Cesa-Bianchi, and R. Garnett, Eds. Curran Associates, Inc., 2018, pp. 3168–3178.
- [7] S. Xiao, J. Yan, X. Yang, H. Zha, and S. M. Chu, "Modeling the intensity function of point process via recurrent neural networks," in *Proceedings of the Thirty-First AAAI Conference on Artificial Intelligence*, ser. AAAI '17. AAAI Press, 2017, pp. 1597–1603.
- [8] S. Xiao, M. Farajtabar, X. Ye, J. Yan, L. Song, and H. Zha, "Wasserstein learning of deep generative point process models," in *Proceedings of the 31st International Conference on Neural Information Processing Systems*, ser. NIPS '17. Red Hook, NY, USA: Curran Associates Inc., 2017, pp. 3250–3259.
- [9] S. Zhu, H. S. Yuchi, and Y. Xie, "Adversarial anomaly detection for marked spatio-temporal streaming data," 2019.
- [10] M.-A. Rizoiu, L. Xie, S. Sanner, M. Cebrian, H. Yu, and P. Van Hentenryck, "Expecting to be hip: Hawkes intensity processes for social media popularity," in *Proceedings of the 26th International Conference on World Wide Web*, 2017, pp. 735–744.
- [11] T. Luong, H. Pham, and C. D. Manning, "Effective approaches to attention-based neural machine translation," in *Proceedings of the 2015 Conference on Empirical Methods in Natural Language Processing*. Lisbon, Portugal: Association for Computational Linguistics, Sep. 2015, pp. 1412–1421.
- [12] A. Vaswani, N. Shazeer, N. Parmar, J. Uszkoreit, L. Jones, A. N. Gomez, L. u. Kaiser, and I. Polosukhin, "Attention is all you need," in *Advances in Neural Information Processing Systems 30*. Curran Associates, Inc., 2017, pp. 5998–6008.
- [13] A. Abadi, T. Rajabioun, and P. A. Ioannou, "Traffic flow prediction for road transportation networks with limited traffic data," *IEEE Transactions on Intelligent Transportation Systems*, vol. 16, no. 2, pp. 653–662, April 2015.
- [14] Y. Lv, Y. Duan, W. Kang, Z. Li, and F. Wang, "Traffic flow prediction with big data: A deep learning approach," *IEEE Transactions on Intelligent Transportation Systems*, vol. 16, no. 2, pp. 865–873, April 2015.
- [15] X. Ma, Z. Dai, Z. He, J. Ma, Y. Wang, and Y. Wang, "Learning traffic as images: a deep convolutional neural network for large-scale transportation network speed prediction," *Sensors*, vol. 17, no. 4, p. 818, 2017.
- [16] Z. Cui, R. Ke, and Y. Wang, "Deep bidirectional and unidirectional LSTM recurrent neural network for network-wide traffic speed prediction," *CoRR*, vol. abs/1801.02143, 2018.
- [17] B. Liao, J. Zhang, C. Wu, D. McIlwraith, T. Chen, S. Yang, Y. Guo, and F. Wu, "Deep sequence learning with auxiliary information for traffic prediction," in *Proceedings of the 24th ACM SIGKDD International Conference on Knowledge Discovery & Data Mining*, ser. KDD '18. New York, NY, USA: Association for Computing Machinery, 2018, pp. 537–546.
- [18] Z. Yuan, X. Zhou, and T. Yang, "Hetero-convlstm: A deep learning approach to traffic accident prediction on heterogeneous spatio-temporal data," in *Proceedings of the 24th ACM SIGKDD International Conference on Knowledge Discovery & Data Mining*, ser. KDD '18. New York, NY, USA: Association for Computing Machinery, 2018, pp. 984–992.
- [19] Y. Gu, W. Lu, X. Xu, L. Qin, Z. Shao, and H. Zhang, "An improved bayesian combination model for short-term traffic prediction with deep learning," *IEEE Transactions on Intelligent Transportation Systems*, pp. 1–11, 2019.
- [20] Z. Pan, Y. Liang, W. Wang, Y. Yu, Y. Zheng, and J. Zhang, "Urban traffic prediction from spatio-temporal data using deep meta learning," in *Proceedings of the 25th ACM SIGKDD International Conference on Knowledge Discovery & Data Mining*, ser. KDD '19. New York, NY, USA: Association for Computing Machinery, 2019, pp. 1720–1730.
- [21] C. Zheng, X. Fan, C. Wang, and J. Qi, "Gman: A graph multi-attention network for traffic prediction," 2019.
- [22] L. Zhu, F. R. Yu, Y. Wang, B. Ning, and T. Tang, "Big data analytics in intelligent transportation systems: A survey," *IEEE Transactions on Intelligent Transportation Systems*, vol. 20, no. 1, pp. 383–398, Jan 2019.
- [23] R. E. Wilson, "An analysis of gipps's car-following model of highway traffic," *IMA journal of applied mathematics*, vol. 66, no. 5, pp. 509–537, 2001.
- [24] A. Zeroual, F. Harrou, Y. Sun, and N. Messai, "Monitoring road traffic congestion using a macroscopic traffic model and a statistical monitoring scheme," *Sustainable cities and society*, vol. 35, pp. 494–510, 2017.
- [25] A. Solé-Ribalta, S. Gómez, and A. Arenas, "A model to identify urban traffic congestion hotspots in complex networks," *Royal Society open science*, vol. 3, no. 10, p. 160098, 2016.
- [26] A. G. Hawkes, "Spectra of some self-exciting and mutually exciting point processes," *Biometrika*, vol. 58, no. 1, pp. 83–90, 1971.
- [27] M. Gomez Rodriguez, J. Leskovec, and A. Krause, "Inferring networks of diffusion and influence," in *Proceedings of the 16th ACM SIGKDD International Conference on Knowledge Discovery and Data Mining*, ser. KDD '10. New York, NY, USA: Association for Computing Machinery, 2010, pp. 1019–1028.
- [28] B. Yuan, H. Li, A. L. Bertozzi, P. J. Brantingham, and M. A. Porter, "Multivariate spatiotemporal hawkes processes and network reconstruction," *SIAM Journal on Mathematics of Data Science*, vol. 1, no. 2, pp. 356–382, 2019.
- [29] S. Zhu and Y. Xie, "Spatial-temporal-textual point processes with applications in crime linkage detection," 2019.
- [30] T. Omi, n. ueda, and K. Aihara, "Fully neural network based model for general temporal point processes," in *Advances in Neural Information Processing Systems 32*. Curran Associates, Inc., 2019, pp. 2120–2129.
- [31] Q. Zhang, A. Lipani, O. Kirnap, and E. Yilmaz, "Self-attentive hawkes processes," 2019.
- [32] G. D. of Transportation, "Traffic analysis and data application (tada)," <http://www.dot.ga.gov/DS/Data>.
- [33] S. Zhu and Y. Xie, "Crime event embedding with unsupervised feature selection," in *2019 IEEE International Conference on Acoustics, Speech and Signal Processing (ICASSP)*, May 2019, pp. 3922–3926.
- [34] OpenStreetMap contributors, "Planet dump retrieved from <https://planet.osm.org>," <https://www.openstreetmap.org>, 2017.
- [35] R. P. Barry and J. M. V. Hoef, "Blackbox kriging: Spatial prediction without specifying variogram models," *Journal of Agricultural, Biological, and Environmental Statistics*, vol. 1, no. 3, pp. 297–322, 1996. [Online]. Available: <http://www.jstor.org/stable/1400521>
- [36] V. Garreta, P. Monestiez, and J. M. Ver Hoef, "Spatial modelling and prediction on river networks: up model, down model or hybrid?" *Environmetrics*, vol. 21, no. 5, pp. 439–456, 2010.
- [37] J. M. V. Hoef, E. Peterson, and D. Theobald, "Spatial statistical models that use flow and stream distance," *Environmental and Ecological Statistics*, vol. 13, no. 4, pp. 449–464, Dec 2006.
- [38] J. M. V. Hoef and E. E. Peterson, "A moving average approach for spatial statistical models of stream networks," *Journal of the American Statistical Association*, vol. 105, no. 489, pp. 6–18, 2010.
- [39] J. Chen, S.-H. Kim, and Y. Xie, "S<sup>3</sup>t: An efficient score-statistic for spatio-temporal surveillance," 2017.
- [40] N. Cressie, J. Frey, B. Harch, and M. Smith, "Spatial prediction on a river network," *Journal of Agricultural, Biological, and Environmental Statistics*, vol. 11, no. 2, p. 127, Jun 2006.
- [41] E. E. Peterson, D. M. Theobald, and J. M. Ver Hoef, "Geostatistical modelling on stream networks: developing valid covariance matrices based on hydrologic distance and stream flow," *Freshwater Biology*, vol. 52, no. 2, pp. 267–279, 2007.
- [42] B. Nitz, "Atlanta breaks 135-year-old rainfall record – and more is on the way," <https://www.ajc.com/news/local/atlanta-breaks-135-year-old-rainfall-record-and-more-the-way/ToXxI0475c7evyvMp2FrMP/>, 2018.
- [43] D. C. Gazis and R. Herman, "The moving and phantom bottlenecks," *Transportation Science*, vol. 26, no. 3, pp. 223–229, 1992.